Conformational Stability and Pathogenic Misfolding of the Integral Membrane Protein PMP22

Jonathan P. Schlebach,[†,‡] Malathi Narayan,[†,§] Catherine Alford,[#] Kathleen F. Mittendorf,[†,‡] Bruce D. Carter,[†,§] Jun Li,[§,∥,⊥] and Charles R. Sanders*[,†,‡]

[†]Department of Biochemistry, [‡]Center for Structural Biology, [§]Vanderbilt Brain Institute, and [∥]Department of Neurology, Vanderbilt University School of Medicine, Nashville, Tennessee 37232, United States

[⊥]Veterans Affairs Tennessee Valley Healthcare System, Nashville, Tennessee 37232, United States

[#]Flow Cytometry Core, Veterans Affairs Tennessee Valley Healthcare System, Nashville, Tennessee 37232, United States

S *Supporting Information*

ABSTRACT: Despite broad biochemical relevance, our understanding of the physiochemical reactions that limit the assembly and cellular trafficking of integral membrane proteins remains superficial. In this work, we report the first experimental assessment of the relationship between the conformational stability of a eukaryotic membrane protein and the degree to which it is retained by cellular quality control in the secretory pathway. We quantitatively assessed both the conformational equilibrium and cellular trafficking of 12 variants of the α-helical membrane protein peripheral myelin protein 22 (PMP22), the intracellular misfolding of which is known to cause peripheral neuropathies associated with Charcot−Marie−Tooth disease (CMT). We show that the extent to which these mutations influence the energetics of Zn(II)-mediated PMP22 folding is proportional to the observed reduction in cellular trafficking efficiency. Strikingly, quantitative analyses also reveal that the reduction of motor nerve conduction velocities in affected patients is proportional to the extent of the mutagenic destabilization. This finding provides compelling evidence that the effects of these mutations on the energetics of PMP22 folding lie at the heart of the molecular basis of CMT. These findings highlight conformational stability as a key factor governing membrane protein biogenesis and suggest novel therapeutic strategies for CMT.
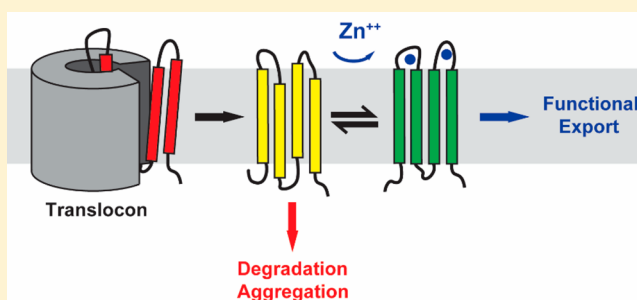
INTRODUCTION

Due to the stringency of cellular quality control (QC), protein production and assembly are often inefficient in the cell. About 30% of newly synthesized proteins in mammalian cells are subject to rapid degradation by proteasomes.[1] However, experimental efforts to rationalize the interplay between the physiochemical properties of polypeptide chains and their interactions with QC networks have thus far been limited to a handful of soluble proteins.[2−7] Far less is known about integral membrane protein folding and assembly,[8] a process that is intimately linked to the molecular basis of numerous diseases.[9−11] Many of the proteins that carry out the QC of nascent integral membrane proteins in the endoplasmic reticulum (ER) have been identified in recent years.[11,12] However, the structural properties subjected to surveillance by QC, potentially triggering disposal by the ER-associated degradation (ERAD) pathway, are largely unexplored. Here we test the hypothesis that the conformational stability of integral membrane proteins plays a central role in their interactions with cellular QC and the efficiency with which they traffic to their intended cellular compartments. To test this hypothesis, we interrogate a series of pathogenic variants of

human peripheral myelin protein 22 (PMP22), the cellular misfolding and misassembly of which causes a spectrum of peripheral neuropathies associated with Charcot−Marie−Tooth (CMT) disease.[8,9,13−15]

PMP22 is expressed in myelinating Schwann cells of the peripheral nervous system (PNS) and is highly abundant in the membranes of compact myelin.[13,16] Strikingly, only 20% of wild-type (WT) PMP22 reaches its intended destination at the plasma membrane under physiological conditions;[17,18] the majority of the nascent protein is retained in the ER and/or targeted for degradation. Furthermore, most pathogenic variants further reduce the trafficking efficiency of PMP22, which suggests that pathogenic mutations promote misfolding within the secretory pathway.[14,19,20] We recently reported quantitative thermodynamic measurements of the conformational stability of purified WT PMP22,[21] the first such measurement to be made for any multispan eukaryotic membrane protein. Surprisingly, we found that WT PMP22 exhibits marginal conformational stability *in vitro*, which
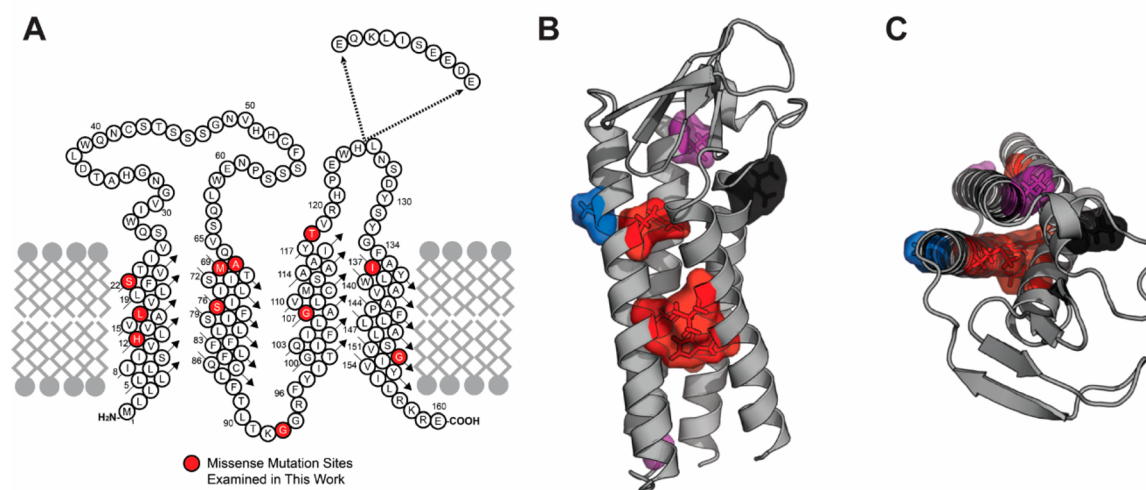
Figure 1. Structural distribution of pathogenic mutations in PMP22. A topology diagram and a structural model depict the positions of the mutated residues and the position of the myc epitope tag that was inserted for immunological detection of PMP22 in mammalian cells. (A) A cartoon depicts the topology of the sequence of PMP22 with respect to the membrane. The positions of the mutated residues characterized herein are indicated in red. The position of the myc epitope tag inserted into the constructs used for cellular trafficking studies is indicated with dashed lines. The lowest-energy conformation of a recently published structural model of the apo-form of PMP22 is viewed parallel to the position of the membrane (B) and from its extracellular face (C),[34] with the positions of the pathogenically mutated side-chains characterized in this work being highlighted for reference. Mutated side chains associated with DSS (severe neuropathy), which include H12Q, L16P, M69K, S76I, and G150D, are shown in red. Mutated side chains associated with CMT disease (CMT1, moderate neuropathy), which include G107V and T118M, are shown in purple. Mutated side chains associated with HNPP (mild neuropathy), which include S22F and A67T, are shown in blue. Finally, the position of the side chain for the nonpathogenic I137V mutation site is shown in black.

Table 1. Stability and Zn(II) Binding of Pathogenic PMP22 Variants[a]

				Zn(II) binding				
variant	disease	f_{fold}	$\Delta\Delta G_{F-U}$ (kcal/mol)	$K_{d1,app}$ (μM)	$\Delta\Delta G_{app1}$ (kcal/mol)	$K_{d2,app}$ (mM)	$\Delta\Delta G_{app2}$ (kcal/mol)	$\Delta\Delta G_{app,total}$ (kcal/mol)
WT	–	0.53 ± 0.06	–	60 ± 50	–	1.9 ± 0.3	–	–
G107V	CMT1	0.66 ± 0.05	−0.33 ± 0.08	[b]	–	2.1 ± 0.2	0.1 ± 0.1	–
T118M	CMT1	0.60 ± 0.01	−0.17 ± 0.06	210 ± 90	0.7 ± 0.6	4.9 ± 0.9	0.6 ± 0.1	1.3 ± 0.6
H12Q	DSS	0.38 ± 0.02	0.37 ± 0.07	410 ± 80	1.1 ± 0.5	16 ± 5	1.3 ± 0.2	2.4 ± 0.6
S22F	HNPP	0.28 ± 0.01	0.62 ± 0.07	410 ± 40	1.1 ± 0.5	10 ± 4	1.0 ± 0.2	2.1 ± 0.6
I137V	–	0.16 ± 0.02	1.0 ± 0.1	140 ± 70	0.4 ± 0.6	1.2 ± 0.6	−0.3 ± 0.3	0.2 ± 0.7
A67T	HNPP	0.10 ± 0.02	1.3 ± 0.1	130 ± 100	0.4 ± 0.7	0.86 ± 0.8	−0.5 ± 0.6	−0.1 ± 0.9
G150D	DSS	0.08 ± 0.02	1.5 ± 0.2	360 ± 90	1.0 ± 0.5	7 ± 2	0.8 ± 0.2	1.8 ± 0.6
M69K	DSS	∼0	>2.0	320 ± 40	1.0 ± 0.5	35 ± 6	1.7 ± 0.1	2.7 ± 0.5
S76I	DSS	∼0	>2.0	500 ± 100	1.2 ± 0.5	30 ± 10	1.7 ± 0.2	2.9 ± 0.6
G93R	CMT1	∼0	>2.0	410 ± 40	1.1 ± 0.5	38 ± 7	1.8 ± 0.2	2.9 ± 0.5
L16P	DSS	∼0	>2.0	700 ± 200	1.4 ± 0.5	46 ± 8	1.9 ± 0.1	3.3 ± 0.5

[a]The fraction of folded protein (f_{fold}) was determined from near-UV CD spectra as detailed in the Experimental Section. $\Delta\Delta G_{F-U}$ values were determined as described in the Experimental Section, with the associated error values reflecting propagated standard deviations. $K_{d,app}$ values represent the globally fit values from three replicate titrations of the protein with ZnCl$_2$ at pH 5.5, with the errors reflecting the standard error of the fitted value. $\Delta\Delta G_{app}$ values were determined as described in the Experimental Section, with the associated error values reflecting propagated standard errors. [b]This value could not be confidently determined by global fitting.

parallels its rapid degradation and inefficient trafficking in the cell. To elucidate the nature of the interplay between the folding and cellular trafficking of integral membrane proteins, we here quantitatively survey the conformational stability and cellular trafficking of a series of misfolding-prone pathogenic PMP22 variants. Remarkably, the results not only appear to confirm a mechanistic linkage between conformational stability and cellular trafficking but also strongly suggest that the degree of mutagenic destabilization is directly related to the severity of peripheral neuropathy in humans carrying the associated mutations in the *PMP22* gene.

■ RESULTS

Selection of Pathogenic Mutations in PMP22. Several of the known pathogenic mutations in the *PMP22* gene have been found to enhance the misfolding and mistrafficking of PMP22 in the cell.[14,22] Therefore, characterization of the effects of these mutations provides an opportunity to elucidate a potential relationship between conformational stability and cellular trafficking. From the 44 known pathogenic missense mutations in *PMP22* associated with peripheral neuropathies (Human Gene Mutation Database, http://www.hgmd.cf.ac.uk/ac/index.php), we selected 10 pathogenic variants and 1 nonpathogenic isoform that are dispersed throughout the 4 transmembrane (TM) helices of PMP22 (Figure 1A). These

mutations cause a spectrum of clinical phenotypes ranging from hereditary neuropathy with liability to pressure palsies (HNPP, mild neuropathy), CMT Type 1 (CMT1, moderate neuropathy), and Dejerine−Sottas syndrome (DSS, severe neuropathy) (Table 1). Previously reported motor nerve conduction velocities of patients harboring these mutations confirm that the degree of dysmyelination caused by these mutations is highly variable (Supplementary Table 1), which suggests that this set of mutations is likely to manifest a range of effects on the conformational equilibrium of PMP22. Additionally, we recently found that none of these mutations are predicted to cause topogenic defects,[23] which suggests that conformational defects are manifested after PMP22 is cotranslationally inserted into the membrane.

Influence of Pathogenic Mutations on the Conformational Stability of the apo-Form of PMP22. We recently characterized the conformational equilibrium of purified WT PMP22 in *n*-dodecylphosphocholine (DPC) micelles and found that only ∼50% of the protein is folded at equilibrium.[21] Because the free energy difference between the folded and unfolded ensembles is minimal under this condition ($\Delta G_{F-U} \sim$ 0 kcal/mol), even small perturbations of the conformational equilibrium caused by mutations should cause measurable differences in the fraction of folded protein. Therefore, to determine the effects of pathogenic mutations on the conformational stability, we assessed the tertiary folding of pathogenic PMP22 variants in DPC micelles at equilibrium using near-UV circular dichroism (CD) spectroscopy, which is sensitive to the tertiary ordering of aromatic side chains. The shapes of the near-UV CD spectra of these variants are similar to that of the WT protein (Figure 2 and Supplementary Figure 1), suggesting that the mutations do not significantly alter the tertiary structure of the folded protein. However, significant
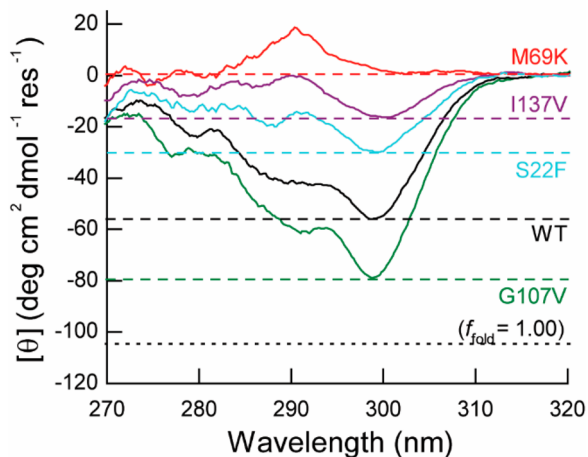
differences are apparent in the magnitude of the tryptophan peak at 299 nm ($[\theta]_{299}$), which reflects the fraction of folded PMP22 (f_{fold}).[21,24] With the exception of G107V and T118M PMP22, $[\theta]_{299}$ is diminished in the spectra of the mutant proteins (Figure 2 and Supplementary Figure 1), which confirms that these mutations reduce f_{fold}. Based on the signal of the folded protein and the signal of the unfolded protein (see Experimental Section), we determined f_{fold} for each mutant variant in DPC micelles directly from the near-UV CD spectra (Table 1). Moreover, because PMP22 achieves conformational equilibrium under these conditions,[21] f_{fold} values can be used to directly determine the free energy of folding (ΔG_{F-U}) and to calculate the effect of a mutation on the free energy of folding ($\Delta\Delta G_{F-U}$). The energetic effects of four of the pathogenic mutations (H12Q, S22F, G107V, and T118M) appear to be modest ($|\Delta\Delta G_{F-U}| < 1.0$ kcal/mol, Table 1). In contrast, four other pathogenic mutations (L16P, M69K, S76I, and G93R) significantly shift the conformational equilibrium toward the unfolded state ($\Delta\Delta G_{F-U} > 2.0$ kcal/mol, Table 1). None of the mutations appear to significantly stabilize PMP22. Furthermore, three of the four highly destabilizing mutations (L16P, M69K, and S76I) are associated with severe pathogenic phenotypes (DSS). Together, these data demonstrate that the majority of the pathogenic mutations studied herein decrease the conformational stability of PMP22. Nevertheless, the fact that the nonpathogenic I137V variant decreases the conformational stability while the severely pathogenic H12Q variant has a negligible effect on the conformational equilibrium of the apoprotein is puzzling. These observations suggest that additional factors, such as the presence of an endogenous ligand, may influence the conformational equilibrium of PMP22 *in vivo*.

Influence of Metal Ion Binding on the Conformational Equilibria of PMP22 Variants. The energetics of protein folding and misfolding in the cell depend on the physiochemical properties of the cellular compartments in which QC occurs.[25] One decisive factor is the concentration of ligands or cofactors,[4] which can bind to and stabilize native conformations relative to misfolded conformations.[26,27] PMP22 is known to have an avid affinity for Zn(II) and Cu(II) and features two divalent cation binding sites,[24] which likely employ the five histidine residues in its extracellular loops (Figure 1A). Given that myelin is rich in both Zn(II) and Cu(II),[28,29] it is highly probable that the binding of metal ion cofactors influences PMP22 folding and assembly within the cell. We therefore sought to compare the influence of metal binding on the conformational equilibrium of WT and mutant PMP22 variants. We first compared the propensity of the destabilized G150D and L16P variants to bind Zn(II) relative to WT using fluorescence spectroscopy, as previously detailed.[24] A gain in the intrinsic tryptophan fluorescence intensity is coincident with consecutive Zn(II) binding events for each of these variants (Figure 3A), which suggests that binding is coupled to the formation of tertiary structure. Importantly, this aspect of the titration data highlights the fact that these proteins are not fully folded in the absence of metal ions (Table 1). Therefore, binding measurements *must* significantly underestimate the true binding affinity. Nevertheless, comparison of the apparent binding affinities provides insight into whether mutations influence Zn(II) binding. Fitting of the titration data with a two-site binding model reveals that these mutations significantly increase both of the apparent equilibrium dissociation constants ($K_{d, app}$) relative to those of WT (Figure 3A, Table

Figure 2. Conformational stability of PMP22 variants. The fraction of folded protein (f_{fold}) was assessed for WT and mutant PMP22 using near-UV CD spectroscopy. The average CD signal from three replicate near-UV CD measurements of WT (black) and four representative mutant variants including S22F (cyan), M69K (red), G107V (green), and I137V (purple) PMP22 under nondenaturing conditions is plotted against the wavelength. The magnitude of the tryptophan peak, which serves as a reliable probe for the fraction of folded PMP22,[21,24] is indicated for each variant with dashed lines. The magnitude of the signal of the fully folded proteins determined from equilibrium unfolding of WT protein in the presence of stabilizing osmolytes (see Experimental Section) is indicated with a dotted line for reference.
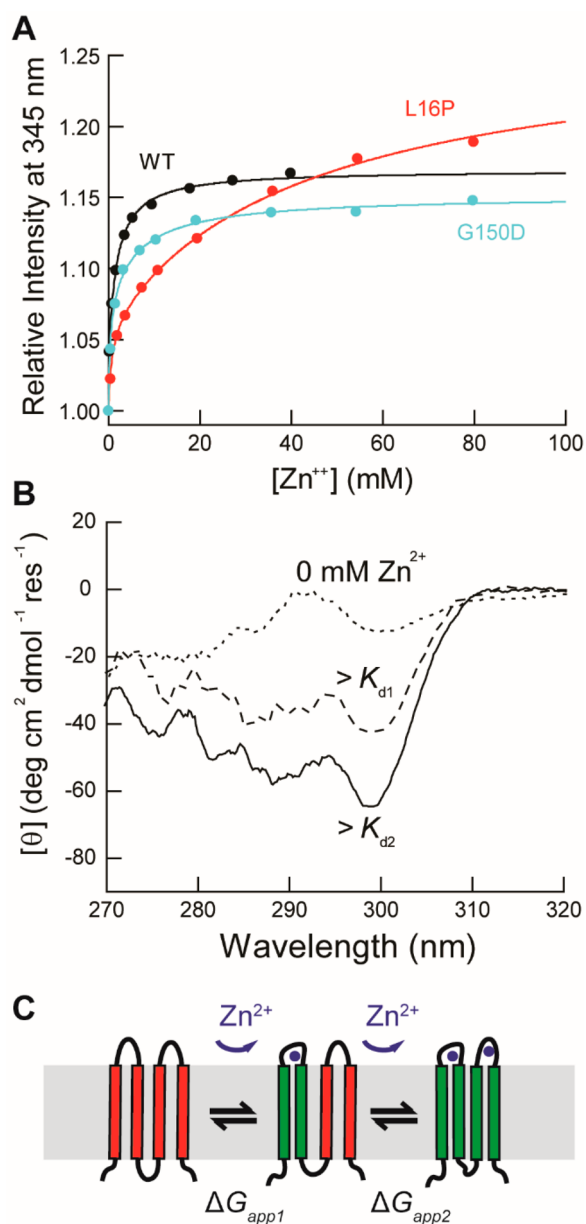
Figure 3. Zinc binding of wild-type and mutant PMP22 variants. Zn(II) binding was monitored for WT and mutant PMP22 variants in DPC micelles at pH 5.5 using near-UV CD and tryptophan fluorescence. (A) WT (black), G150D (cyan), and L16P (red) PMP22 were titrated with ZnCl₂, and binding was monitored by the change in the intensity of the tryptophan fluorescence emission at 345 nm. The relative fluorescence intensity at 345 nm from representative replicate experiments is plotted against the concentration of ZnCl₂, and the global fit of each data set to a two-site binding model is shown. (B) G150D PMP22 was equilibrated in the presence of 0 mM (dotted line), 720 μM ($2 \times K_{d1,app}$, dashed line), and 14 mM ($2 \times K_{d2,app}$, solid line) ZnCl₂ prior to measurement of the near-UV CD spectra, and the mean residue ellipticity ($[\theta]$) is plotted against the wavelength. (C) A cartoon depicts a hypothetical reaction coordinate for the coupled binding and folding of the G150D PMP22 variant.

1). These findings confirm that pathogenic mutations interfere with the formation of Zn(II)-bound PMP22.

To assess the nature of the structural changes that occur upon binding, we used near-UV CD to probe the tertiary structure of the bound forms of G150D PMP22, which is mostly unfolded in DPC micelles at equilibrium in the absence

of Zn(II) (Figures 3B and Supplementary Figure 1). The addition of a two-fold excess of Zn(II) relative to the first apparent equilibrium dissociation constant ($K_{d1,app}$) of G150D PMP22 is coincident with an increase in the near-UV CD signal at 299 nm (Figure 3B). However, despite the fact that 67% of the protein is saturated with a single Zn(II) ion under this condition, only about 37% of the native CD signal is recovered. This result demonstrates that the saturation of the first binding site is coupled to a *partial* folding reaction. A second folding reaction occurs upon saturation of the second binding site. In the presence of a two-fold excess of Zn(II) relative to the second apparent equilibrium dissociation constant ($K_{d2,app}$) (a condition under which 67% of the protein is bound to two Zn(II) ions), approximately 57% of the native CD signal is recovered (Figure 3B). The similarity between the fraction of doubly bound protein and the apparent fraction of folded protein under this condition suggests that saturation of both binding sites is thermodynamically coupled to *global* folding. Though we previously found no evidence for the accumulation of partially folded equilibrium intermediates in the absence of metal ions,[21] these results clearly show that at least three conformational states accumulate during coupled Zn(II) binding and folding (Figure 3C). Together, these findings confirm that metal ion binding is thermodynamically coupled to PMP22 folding.

Elucidation of the effects of pathogenic mutations on the energetics of coupled binding and folding reactions may provide insight into the mechanism by which mutations in PMP22 prompt cellular misfolding. Unambiguous delineation of the effects of mutations on binding and folding would require equilibrium unfolding measurements in the presence of metal ions. However, such measurements cannot be achieved because the negatively charged detergents utilized as denaturing agents for α-helical membrane proteins form insoluble complexes with divalent metal ions.[30] Nevertheless, because binding is thermodynamically coupled to refolding, changes in the apparent equilibrium dissociation constants ($K_{d,app}$) quantitatively reflect the effects of mutations on the energetics of the overall binding and folding reaction. The effect of a mutation on the apparent free energy difference associated with this cooperative binding and folding reaction ($\Delta\Delta G_{app}$) can therefore be expressed as follows:

$$\Delta\Delta G_{app} = -RT \ln \frac{K_{d,app\,WT}}{K_{d,app\,mut}} \tag{1}$$

where R is the gas constant, T is the temperature, $K_{d,app\,wt}$ is the apparent equilibrium dissociation constant of the wild-type protein, and $K_{d,app\,mut}$ is the apparent equilibrium dissociation constant of the mutant protein. Summing $\Delta\Delta G_{app}$ values for the two sequential binding and folding reactions therefore yields the effect of a mutation on the free energy difference between the apoprotein ensemble and the globally folded Zn(II)-bound form of PMP22 ($\Delta\Delta G_{app,total}$) as follows:

$$\Delta\Delta G_{app,total} = -RT \ln \frac{K_{d1,app\,WT} K_{d2,app\,WT}}{K_{d1,app\,mut} K_{d2,app\,mut}} \tag{2}$$

which reflects the energetic effects of mutations on the formation of the fully folded Zn(II)-bound form of PMP22.

The energetic effects of the G150D ($\Delta\Delta G_{app,total} = 1.8 \pm 0.6$ kcal/mol) and L16P ($\Delta\Delta G_{app,total} = 3.3 \pm 0.5$ kcal/mol) mutations on the formation of Zn(II)-bound PMP22 are consistent with the magnitude by which these mutations

destabilize the apoprotein ($\Delta\Delta G_{F-U}$ = 1.5 ± 0.2 and >2.0 kcal/mol for the G150D and L16P, respectively) (Table 1), indicating that these mutations likely disrupt similar contacts present in both the apoprotein and in the Zn(II)-bound forms. We surveyed the additional nine mutations studied herein for their energetic effects on the formation of Zn(II)-bound PMP22. With the exception of S22F, which exhibits a unique decrease in intrinsic tryptophan fluorescence upon saturation of its second binding site (Supplementary Figure 2), a similar increase in the intrinsic tryptophan fluorescence coincided with binding and folding for each variant, which suggests similar structural rearrangements occur upon Zn(II) binding. Interestingly, the degree to which these mutations influence the energetics of binding and folding ($\Delta\Delta G_{app,total}$) is in several cases distinct from the degree to which they destabilize the apoprotein ($\Delta\Delta G_{F-U}$) (Table 1). For instance, despite the fact that the apoprotein form of the nonpathogenic I137V variant is destabilized relative to the WT protein ($\Delta\Delta G_{F-U}$ = 1.0 ± 0.1 kcal/mol), the energetics of binding and folding for I137V PMP22 are indistinguishable from that of WT PMP22 ($\Delta\Delta G_{app,total}$ = −0.1 ± 0.9 kcal/mol). In contrast, the severely pathogenic H12Q mutation has minimal influence on the conformational stability of the apoprotein ($\Delta\Delta G_{F-U}$ = 0.37 ± 0.07 kcal/mol) but significantly destabilizes the Zn(II)-bound form of PMP22 ($\Delta\Delta G_{app,total}$ = 2.4 ± 0.6 kcal/mol). Overall nine of the ten pathogenic mutations surveyed disrupt the formation of Zn(II)-bound PMP22 to a significant extent ($\Delta\Delta G_{app,total}$ > 1.0 kcal/mol), with all four of the mutations responsible for severe disease (DSS) exhibiting the largest energetic effects on the formation of Zn(II)-bound PMP22. These results demonstrate that pathogenic mutations exhibit differential effects on the apoprotein and Zn(II)-bound forms of PMP22 and suggest the effects of the mutations on the bound form may be more closely related to the pathogenic misfolding mechanism.

Quantification of the Cellular Trafficking Efficiency of Pathogenic PMP22 Variants. To assess the linkage between the destabilization imparted by these mutations and the mechanisms of pathogenic cellular misfolding, we sought to relate *in vitro* folding measurements to the degree with which these variants are retained by cellular QC. Recognition of misfolded PMP22 by cellular QC machinery is a key factor leading to the retention of pathogenic variants in the secretory pathway and the decrease in the concentration of mature PMP22 at the plasma membrane.[14,19,22,31−33] We therefore devised a means to quantitatively assess the efficiency with which these variants escape QC and traffic to the plasma membrane. PMP22 variants were transiently expressed in Madin−Darby canine kidney (MDCK) cells, and PMP22 at the plasma membrane was then labeled with a PE-conjugated primary antibody. To detect retained intracellular PMP22, the cells were then fixed, permeabilized, and again immunostained with an Alexa Fluor 647-conjugated primary antibody. Flow cytometry was then employed to quantify the immunostaining of PMP22 at the plasma membrane (folded) and in the intracellular compartments (misfolded) for each cell. Single-cell trafficking efficiencies were then calculated based on cellular fluorescence profiles. Cells expressing WT PMP22 consistently exhibited significant trafficking of the protein to the plasma membrane (Figure 4A), though its trafficking efficiency varied considerably across the cellular population (Figure 4B). The population average for WT PMP22 (17 ± 3%) is consistent with previously reported estimates of the WT PMP22
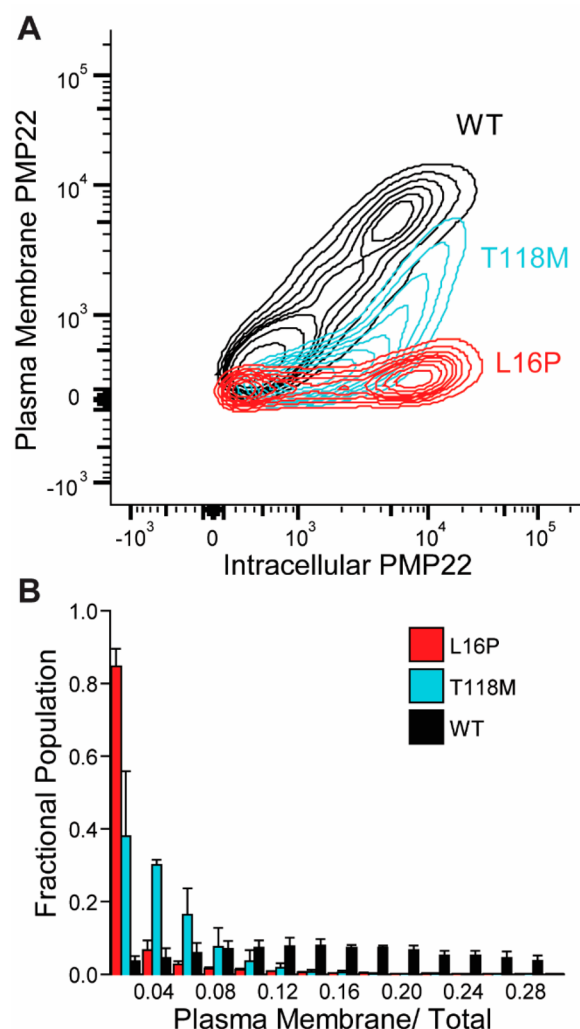

Figure 4. Cellular trafficking of PMP22 variants in MDCK cells. WT and mutant PMP22 variants were transiently expressed in MDCK cells, and the cellular trafficking of these proteins was quantitatively assessed using flow cytometry. (A) Contour plots depict the distribution of 2500 GFP-positive cells from a representative flow cytometry experimental replicate expressing WT (black), T118M (cyan), or L16P (red) PMP22 according to their relative immunostaining of PMP22 at the plasma membrane (stained with a PE-conjugated monoclonal antibody) and intracellular PMP22 (stained with an Alexa Fluor 647-conjugated monoclonal antibody). (B) A histogram depicts the fraction of the cellular population with the indicated ratio of the staining of PMP22 at the plasma membrane to that of the total PMP22 staining for cells expressing WT (black), T118M (cyan), or L16P (red) PMP22. Calculated ratios account for both the effect of nonspecific binding of the antibodies as well as the intrinsic difference in the intensities of the signal of the two fluorescently labeled antibodies (see Experimental Section). The heights of the bars reflect the average fractional population from three replicate experiments (7500 cells total per variant) and the error bars reflect the standard deviations of these values.

trafficking efficiency in Schwann cells (∼20%).[18] Furthermore, the relative trafficking efficiencies of pathogenic variants (Table 2) are generally consistent with previous qualitative observations in other cell lines.[14,19] The trafficking efficiencies of the nonpathogenic I137V PMP22 and those of the S22F and A67T variants associated with mild disease phenotypes are quite similar to that of the WT protein (Table 2). However, the other

Table 2. Cellular Trafficking of Pathogenic PMP22 Variants in MDCK Cells[a]

variant	disease	relative total intensity	relative PM Intensity	trafficking efficiency (%)
WT	–	1	1	17 ± 3
S22F	HNPP	1.4 ± 0.1	2.0 ± 0.1	22 ± 6
I137V	–	0.81 ± 0.03	0.78 ± 0.05	17 ± 2
A67T	HNPP	1.0 ± 0.2	0.81 ± 0.03	13 ± 4
G93R	CMT1	0.7 ± 0.1	0.42 ± 0.02	9 ± 2
T118M	CMT1	1.0 ± 0.2	0.29 ± 0.02	4 ± 1
M69K	DSS	1.0 ± 0.2	0.11 ± 0.01	2.9 ± 0.9
L16P	DSS	1.2 ± 0.3	0.062 ± 0.004	1.4 ± 0.4
G150D	DSS	1.3 ± 0.4	0.032 ± 0.004	0.9 ± 0.1
S76I	DSS	1.2 ± 0.3	0.030 ± 0.004	0.6 ± 0.2
H12Q	DSS	1.2 ± 0.2	0.029 ± 0.006	0.6 ± 0.2
G107V	CMT1	1.2 ± 0.3	0.027 ± 0.002	0.6 ± 0.2

[a]Values represent the average of three replicate population-averaged values (2,500 GFP-positive cells per replicate), and errors reflect the standard deviation of the population-averaged values.

eight pathogenic variants exhibit markedly decreased trafficking efficiencies (Figure 4, Table 2). Considering that total cellular PMP22 expression levels were comparable for all variants tested (Table 2), these differences likely reflect the degree of cellular misfolding and the resulting intracellular retention by the cellular QC machinery. Importantly, five of the six variants with the highest degree of intracellular retention are highly destabilized and are associated with severe disease phenotypes. These observations quantitatively affirm the notion that a reduction in cellular trafficking is a common effect of pathogenic mutations[9,14] and suggests that the intracellular retention of pathogenic PMP22 variants is related to their reduced conformational stability.

Relationships between Conformational Stability, Trafficking Efficiency, and Dysmyelination. To our knowledge, the relationship between the conformational stability of an α-helical membrane protein and its cellular trafficking in mammalian cells has not been previously explored. Our observations are generally suggestive of a relationship between folding and export. Notably, most highly destabilized proteins exhibit reduced trafficking (Tables 1 and 2). However, there are two exceptions. The S22F mutant PMP22 exhibits a unique increase in its cellular trafficking efficiency, which may be related to the distinct structural properties of the Zn(II)-bound form of S22F PMP22 (Supplementary Figure 2). Also, the G107V variant appears to have comparable conformational stability to that of WT PMP22 (Table 1), yet exhibits impaired cellular trafficking (Table 2). However, we noticed that the intrinsic tryptophan fluorescence intensity of G107V PMP22 is similar to that of WT PMP22 under our experimental conditions, which has been optimized for biophysical studies, but greatly diminished at physiological pH (Supplementary Figure 3). This finding suggests the structural defects caused by this particular mutation may not be manifested under the conditions used for our folding reactions. For these reasons, we have excluded the S22F and G107V variants from our analysis of the relationship between the conformational stability and cellular trafficking of PMP22 variants.

In order to assess the mechanism of pathogenic cellular misfolding, we compared the conformational stability and cellular trafficking measurements. We first plotted $\Delta\Delta G_{F-U}$ values for the folding of the PMP22 apoprotein against relative

degree of plasma membrane trafficking but found no apparent relationship (Supplementary Figure 4). In contrast, a linear relationship is apparent between the energetic effects of mutations on Zn(II)-mediated PMP22 folding ($\Delta\Delta G_{app,total}$) and the degree of plasma membrane trafficking ($R^2 = 0.73$, Figure 5A). A key feature of this correlation is the differentiation of pathogenic phenotypes that arises from these combined measurements: mutations that cause severe disease phenotypes (DSS) exhibit the highest degree of destabilization and the largest reduction in cellular trafficking, while mutations that cause moderate to mild phenotypes (CMT1 and HNPP) have more subtle effects. This correlation has critical implications for the role of metal ions as PMP22 cofactors. To further examine the relationship between binding, folding, and trafficking, we corrected the apparent Zn(II) binding constants for differences in the stabilities of the variants (Supplemental Theory). Simulations based on corrected thermodynamic parameters confirm Zn(II) binding represents a key mediator of the folding equilibrium constant and cellular trafficking of PMP22 (Supplemental Theory). Together these findings strongly suggest that pathogenic misfolding arises as a result of the impact of mutations on the Zn(II)-binding-linked conformational stability of PMP22.

We next sought to determine whether these observations are also consistent with the degree of dysmyelination arising from these mutations. Because myelin principally provides insulation for nerve axons to enhance conductance, pathogenic dysmyelination in CMT1 and related disorders reduce motor nerve conduction velocities (NCV). NCV values for patients who are heterozygous for the mutations studied in this work therefore represent a favorable metric for the severity of the disease phenotype. A striking linear correlation ($R^2 = 0.88$) is apparent between NCV values and the relative concentrations PMP22 variants at the plasma membrane (Figure 5B), which strongly supports the notion that the mistrafficking of PMP22 variants represents a key pathogenic mechanism leading to dysmyelination. Furthermore, NCV values are also correlated with the energetic effects of these mutations on Zn(II)-mediated PMP22 folding ($R^2 = 0.64$, Figure 5C), suggesting that the compromised stability of the Zn(II)-bound forms of these variants is responsible for their aberrant trafficking *in vivo* and, ultimately, for dysmyelination. Together, these findings indicate that the conformational instability of PMP22 underlies most neuropathies arising from pathogenic missense mutations in the *PMP22* gene.

■ DISCUSSION

Collectively, our results suggest that metal ion-mediated folding is a limiting reaction within the PMP22 biosynthetic pathway. These findings strongly suggest that conformational stability is a critical variable in the proper production and cellular trafficking of integral membrane proteins in the cell; a finding with broad relevance to the molecular basis of a number of diseases.[8] Furthermore, we believe these results serve to unify a number of observations involving pathogenic PMP22 variants and have implications for the rational design of novel therapeutics for this class of hereditary peripheral neuropathies.

Physiochemical Basis for the Pathogenic Misfolding of PMP22 Variants. We recently found that the positions of pathogenically mutated side chains associated with severe disease phenotypes almost all fall within the protein core of a structural model of the PMP22 apoprotein (Figure 1B,C), suggesting that pathogenic misfolding may principally arise as a
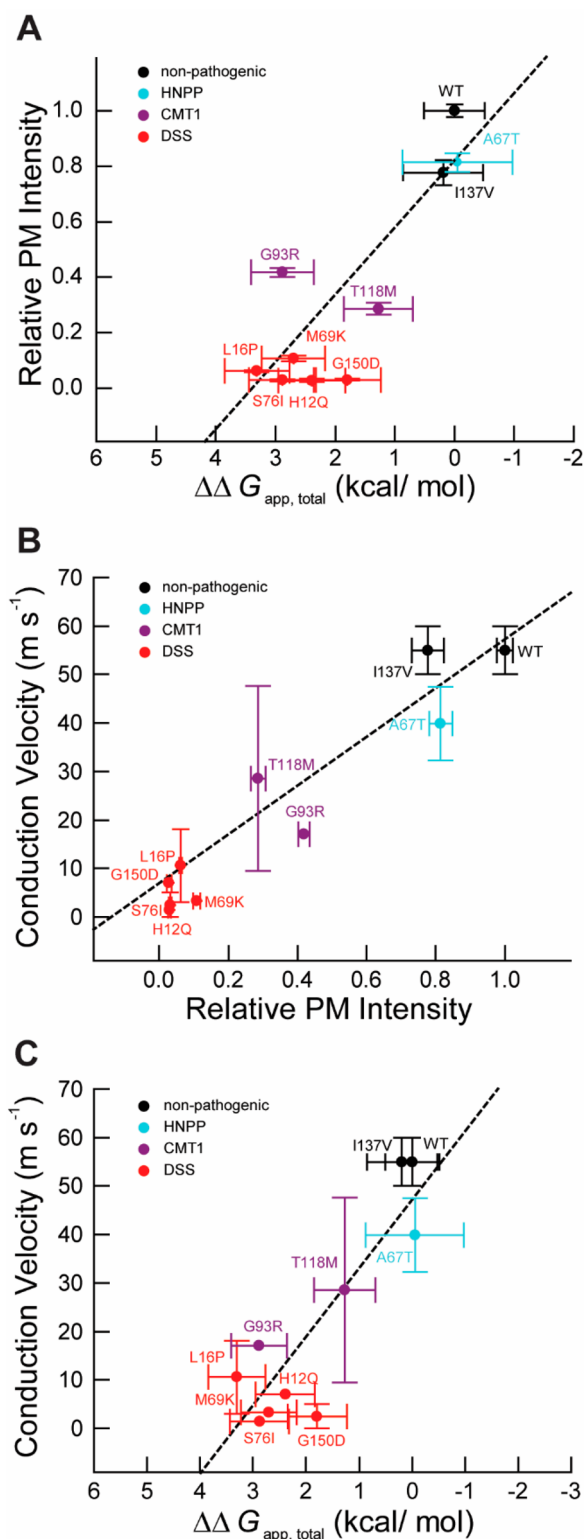
Figure 5. continued

experimental errors ($R^2 = 0.73$) is shown (dashed line). Variants are color coded based on the classification of the corresponding disease phenotypes. (B) Motor nerve conduction velocities (NCV) of patients harboring pathogenic mutations (Supplementary Table 1) were plotted against the relative surface immunostaining of MDCK cells expressing the corresponding PMP22 variant (Table 2). An unweighted linear fit of the data ($R^2 = 0.88$) is shown (dashed line). Variants are color coded based on the classification of the corresponding disease. (C) NCVs from patients harboring pathogenic mutations in PMP22 (Supplementary Table 1) were plotted against the $\Delta\Delta G_{app,total}$ values of the corresponding PMP22 variant (Table 1). An unweighted linear fit of the data ($R^2 = 0.64$) is shown (dashed line). Variants are color coded based on the classification of the corresponding disease.

result of the disruption of tertiary contacts within the native structure.[34] While the findings of this paper are generally consistent with this notion, the results also highlight metal ion binding as a factor that likely contributes to the net conformational stability of PMP22 under physiological conditions (Figure 5A,C). The conformational stability of PMP22 *in vivo* should therefore depend both on the intrinsic conformational stability of the apoprotein and the metal ion binding affinity. Inspection of the folding data and binding data reveals that pathogenic mutations can destabilize the protein by interfering with helical packing, metal ion binding, or both (Table 1). Regardless of the destabilization mechanisms, the net energetic effect of these mutations on the formation of the fully folded, Zn(II)-bound PMP22 is clearly important for its cellular trafficking (Figure 5A) and the degree of dysmyelination (Figure 5C). The notion that metal ions play a critical role in PMP22 biogenesis is quite reasonable considering the essential roles metal ions play in the nervous system. Zinc and copper are plentiful in myelin,[28,29] and depletion of either results in peripheral neuropathy.[35−37] Moreover, compaction of PNS myelin has been shown to be mediated by Zn(II)[38] and other Zn(II)/Cu(II) binding proteins expressed in myelin such as the myelin basic protein.[39−41] Based on our results, we hypothesize that the binding of metal ions likely constitutes one of the decisive interactions in the biosynthetic pathway of PMP22. Such a role for metal ions in PMP22 biogenesis is fully consistent with emerging perspectives on the influence of metabolites and cofactors on the rate and efficiency of protein folding in the cell.[4,25−27,42]

This work confirms the long-held suspicion that the conformational stability of PMP22 is intimately linked to its cellular fate.[9,21,24,43] Considering that passage through QC involves a large number of diverse protein−protein, protein−metabolite, and protein−lipid interactions,[26,27] it is remarkable that such simple relationships are apparent. Nevertheless, it should be noted that a similar empirical linear relationship has previously been documented between the conformational stabilities of mutant forms of a water-soluble protein (bovine pancreatic trypsin inhibitor) and their secretion efficiencies.[2,3] Such relationships suggest that the structural defects detected by QC are closely linked to conformational stability. Differences in the folding and/or unfolding kinetics, for example, may underlie differential recognition unstable variants.[4,26,27] In this regard, it should be noted that PMP22 folding, which requires hours to reach equilibrium *in vitro*,[21] is accelerated roughly 30-fold in the presence of Zn(II) (Supplementary Table 2). The increase of the folding rate of binding-competent variants by

Figure 5. Correlation of Zn(II) binding energetics and cellular trafficking of PMP22 variants to clinical phenotypes. Correlations between the quantitative effects of mutations on the apparent free energy of Zn(II) binding ($\Delta\Delta G_{app,total}$), the quantitative effects of mutations on the cellular trafficking of PMP22, and the motor nerve conduction velocities of patients with the corresponding mutations are shown. (A) The surface-immunostaining of MDCK cells expressing PMP22 variants were normalized relative to that of the WT protein (Table 2) and plotted against the corresponding $\Delta\Delta G_{app,total}$ values (Table 1). A linear fit of the data weighted according to the

metal ions may, in turn, prevent the formation of interactions of between PMP22 and various folding sensors such as calnexin,[9] which is known to form long-lived interactions with destabilized PMP22 variants.[31,32,44] Further studies are needed to gain mechanistic insight into the key interactions that limit the folding and trafficking of PMP22 in cells.

PMP22 Misfolding and the Molecular Basis of Charcot–Marie–Tooth Disease. The apparent relationships between folding, trafficking, and NCV values in patients harboring these mutations suggest the decreased yield of folded PMP22 at the plasma membrane constitutes the key driver of dysmyelination in the afflicted patients (Figure 5B,C). However, the etiology of CMT1 and related peripheral neuropathies is believed to stem from a variety of biochemical effects of pathogenic PMP22 mutations including the enhanced retention of pathogenic variants in the early secretory pathway,[14,19] wild-type/mutant heterodimerization,[22] the formation of intracellular aggregates,[15,33,45,46] and a diminished capacity of the cellular proteostasis network.[45,47] These outcomes likely reflect secondary effects of the misfolding of destabilized PMP22 variants. For instance, the enhanced retention of pathogenic variants in the secretory pathway and the concomitant decrease in the yield of PMP22 at the plasma membrane likely arise as a result of enhanced interactions between misfolded variants and ER chaperones/folding sensors.[31,32,44] Formation of non-native dimers,[22] in turn, may form as a consequence of the buildup of misfolded variants in the endoplasmic reticulum. Polyubiquitination and extrusion of misfolded variants from the ER eventually result in the buildup of large, insoluble aggresomes in the cytosol that are engaged by proteasomal and lysosomal machinery.[46,48] The association of chaperones, proteasomes, and lysosomes with aggresomes coincides with decreases in the buffering capacity of the cellular proteostasis network,[27,47] which may in turn facilitate the secondary aggregation of unrelated proteins that rely on common chaperones. Thus, pharmacological strategies aimed at suppressing the misfolding of pathogenic PMP22 variants could potentially abrogate the chain of events collectively responsible for dysmyelination.

This perspective provides a source of optimism regarding the potential utility of small molecule "pharmacological chaperones" that suppress misfolding by specifically binding the native fold relative to misfolded conformations.[49] Such pharmacological chaperones have been reported for a number of other disease-linked membrane proteins including the cystic fibrosis transmembrane conductance regulator (CFTR) and various G protein-coupled receptors.[50,51] Indeed, the coupling of Zn(II) binding and folding observed for PMP22 in this work demonstrates the feasibility of ligand-mediated PMP22 stabilization. Collectively, these findings indicate that PMP22 represents a promising candidate for the development of pharmacological chaperones.

Pathogenic Misfolding and Mistrafficking of Integral Membrane Proteins. Studies of the biophysical basis of membrane protein misfolding are in an early stage of development. Our findings suggest that the intrinsic thermodynamic preference for the native conformation over a competing ensemble of disordered conformations represents a decisive factor in PMP22 biogenesis. A long line of evidence suggests these principles may extend to a number of other membrane proteins implicated in disease. First, as is true for PMP22 and various other membrane proteins known to undergo misfolding including rhodopsin,[52] CFTR,[53] and the vasopressin V2

receptor,[54] pathogenic mutations generally appear to be evenly distributed throughout the primary sequence. This suggests that pathogenic loss of function most often occurs as a result of misfolding rather than disruption of specific functional elements.[9] Additionally, many of these mutations involve nonconservative substitutions that would be expected to perturb native conformations. For example, pathogenic mutations often involve the introduction of helix-breaking residues, polar residues, or charged residues within TM helices.[55,56] The putative destabilization imparted by such pathogenic substitutions has been previously suggested based on various computational studies[34,57,58] and from biophysical studies of isolated TM helices.[59,60] This work represents the first definitive evidence directly linking conformational destabilization of a human membrane protein to pathogenic cellular misfolding, which opens the door for additional mechanistic investigations of this phenomenon in other related disease-linked integral membrane proteins.

■ CONCLUSION

Despite growing appreciation of protein misfolding as the molecular basis of for numerous diseases, we are just beginning to understand the critical factors that prompt the misassembly of nascent membrane proteins. The linkage documented herein between the conformational stability of an α-helical membrane protein and its passage through cellular QC is likely to be generally applicable to many other membrane proteins implicated in disease and provides fundamental insight into the logic of membrane protein QC in the ER. Our results also strongly suggest a critical role for divalent metal ions in PMP22 biogenesis. Finally, PMP22 appears to be a suitable target for the development of pharmacological chaperones to treat certain forms of CMT1 and related neuropathies.

■ EXPERIMENTAL SECTION

Cloning. Quickchange mutagenesis was used to create mutants of PMP22 within the pAH13 construct, which has been previously described for the expression of PMP22 in *Escherichia coli*.[21,61] For transient expression of PMP22 in mammalian cells, human PMP22 cDNA was subcloned into a pIRES2 vector. This construct expresses PMP22 and EGFP off of the same transcript, which enables facile identification of transformed cells expressing PMP22. Due to the lack of high-quality monoclonal antibodies for PMP22, we used Quickchange mutagenesis to insert a myc epitope into the second extracellular loop of PMP22 within the pIRES2 constructs to enable immunological detection. It has previously been shown that this modification does not impact the trafficking or turnover of the protein.[22,62] Quickchange mutagenesis was also used to introduce point mutations into the pIRES2 vectors prior to purification of each vector using a PerfectPrep EndoFree Plasmid Maxi Kit (5PRIME, Gaithersburg, MD).

Expression and Purification in *E. coli*. WT PMP22 was expressed in *E. coli* and purified as previously described.[21] Expression and purification of mutant proteins were also performed as previously described for the WT protein, except that the mutant proteins were separated from the cleaved expression tag and protein aggregates by cation exchange chromatography using a 1 mL HiTrap SP Sepharose column and/or size exclusion chromatography using a 24 mL Superpose 6 column on an ÄKTA FPLC (GE healthcare, Piscataway, NJ) when necessary.

Stability Measurements. We previously demonstrated that WT PMP22 is only ∼50% folded ($\Delta G_{F-U} \sim 0$ kcal/mol) at equilibrium in DPC micelles,[21] which implies the fraction of folded protein (f_{fold}) should be sensitive to the effects of mutations on the conformational stability under these conditions. Therefore, we directly assessed the f_{fold} of each variant in DPC micelles using near-UV CD spectroscopy

in order to determine the corresponding free energy of folding (ΔG_{F-U}). To measure the f_{fold} for each variant, we assessed the mean residue ellipticity at 299 nm ($[\theta]_{299}$), which serves as a reliable probe for the degree of tertiary structure formation,[21,24] of each variant in nondenaturing DPC micelles and subtracted the signal of the denatured protein in mixed micelles containing DPC and a high mole fraction of the denaturing detergent n-lauroyl sarcosine (LS) (X_{LS}) and then divided this quantity by the signal of the fully folded protein as described below.

Each purified variant protein was equilibrated at room temperature in 25 mM sodium acetate (pH 5.5) containing 150 mM NaCl, 1.0 mM TCEP, and 28 mM DPC (0.00 X_{LS}) prior to acquisition of the near-UV CD spectrum of the protein under nondenaturing conditions using a Jasco J-810 spectropolarimeter (Jasco, Easton, MD). Purified variants were also equilibrated at room temperature in 25 mM sodium acetate (pH 5.5) containing 150 mM NaCl, 1.0 mM TCEP, 28 mM DPC, and 28 mM LS (0.50 X_{LS}), a condition under which the tertiary structure of the WT protein is known to be denatured.[21] The CD spectrum of the denatured protein was then acquired. CD spectra for both the folded protein and the denatured protein were corrected by subtracting the spectra of 25 mM sodium acetate (pH 5.5) containing 150 mM NaCl, 1.0 mM TCEP, and 28 mM DPC (0.00 X_{LS}) (nondenaturing conditions) or of 25 mM sodium acetate (pH 5.5) containing 150 mM NaCl, 1.0 mM TCEP, 28 mM DPC, and 28 mM LS (0.50 X_{LS}) (denaturing conditions), respectively. To minimize the influence of slight deviations in the spectral baselines, all spectra were empirically normalized based on the average signal between 320 and 330 nm, which was observed to be close to zero in all cases. To determine the signal of the folded variant protein from these spectra, the average $[\theta]_{299}$ value from three replicate CD spectra of the denatured protein (at 0.50 X_{LS}), which represents the baseline signal of the fully unfolded protein, was subtracted from the average $[\theta]_{299}$ value of the protein under nondenaturing conditions (0.00 X_{LS}). To determine the f_{fold} value of the variant, this corrected signal was then divided by -105 ± 2 deg cm^2 dmol^{-1} res^{-1}, which is the average signal of the fully folded protein as determined from the fitting of three replicate WT PMP22 equilibrium unfolding transitions measured in the presence of 15% glycerol using a two-state equilibrium model; see ref 21. The f_{fold} values were then used to calculate equilibrium constants and the free energy of folding (ΔG_{F-U}) assuming a two-state equilibrium, which was previously shown to adequately describe the behavior of the WT protein under these conditions at equilibrium.[21]

Zinc Binding Measurements. Zn(II) binding measurements for PMP22 were performed as described previously.[24] Briefly, purified PMP22 variants were equilibrated at a protein concentration of 1 μM at room temperature in 25 mM sodium acetate (pH5.5) containing 150 mM NaCl and 28 mM DPC for at least 1 h prior to binding measurements. The solution was then equilibrated in a quartz cuvette containing a stir bar at 25 °C for at least 15 min prior to serial titration with a stock Zn(II) solution containing 25 mM sodium acetate (pH 5.5), 150 mM NaCl, and 550 mM ZnCl$_2$ using a Hamilton syringe (Reno, NV). Final concentrations ranging from 40 to 80 mM ZnCl$_2$ were achieved, depending on the variant, in order to ensure saturation of both binding pockets. The binding reaction was allowed to proceed for 5 min after each addition, which was judged to be sufficient for the binding kinetics of WT and mutant PMP22 (Supplementary Table 2). The extent of binding was then monitored with a 20 s average of the fluorescence emission intensity at 345 nm with a Jobin Yvonne fluoromax SPEX-3 (Horiba Scientific, Edison New Jersey, NJ). The signal was then corrected according to the dilution factor, and the gain in the fluorescence intensity was normalized relative to the fluorescence intensity of PMP22 in the absence of ZnCl$_2$. The background fluorescence was judged to be negligible according to titrations performed in the absence of PMP22. Binding isotherms were best described by a two-site binding model as judged by the residuals of the fits of the data to single- and two-site binding models. To reduce the influence of random errors on the fitted K_d values, three replicate binding isotherms were globally fitted to determine the two K_d values.

Flow Cytometry. MDCK cells, which have proven to be robust in previous studies of the cellular trafficking of integral membrane proteins,[63] were grown at 37 °C and 5% CO$_2$ in F-12 DMEM containing 10% fetal bovine serum (FBS), penicillin, and streptomycin (Life Technologies, Grand Island, NY) to 20−50% confluency in 6 cm culture dishes. The cells were then transfected in OptiMEM media (Life Technologies, Grand Island, NY) for 24 h with 1 μg of plasmid per dish using effectine transfection reagent (Qiagen, Venlo, NL). The transfection media was then removed, and the cells were allowed to grow in F-12 DMEM containing 10% FBS, penicillin, and streptomycin for an additional 24 h. Transfected cells were trypsinized and prepared for FACS analysis using the Fix & Perm kit in accordance with the manufacturer's instructions (Life Technologies, Grand Island, NY). Briefly, half of the cells from a confluent 6 cm culture dish (ca. 1.6×10^6 cells) were suspended in 100 μL of culture media, and a PE-labeled monoclonal anti-myc antibody (clone 9E10) (Cell Signaling Technology, Danvers, MA) was added to the solution to a final concentration of 0.75 μg/mL to immunostain PMP22 on the surface of the cell. The cells were then incubated in the dark at room temperature for 30 min. 100 μL of the fixation solution was then added to the media, and the cells were incubated for 15 min in the dark at room temperature. The cells were then rinsed and pelleted by centrifugation twice with 3 mL of PBS containing 5% FBS and 0.1% NaN3 (rinse solution). The cells were then suspended in 100 μL of the permeabilization solution, and an Alexa Fluor 647-labeled monoclonal anti-myc antibody (clone 9E10) (Cell Signaling Technology, Danvers, MA) was added to the solution to a final concentration of 0.75 μg/mL to label intracellular PMP22. After a 30 min incubation in the dark at room temperature, the cells were again rinsed and pelleted by centrifugation twice using rinse solution then resuspended in 300 μL of the rinse solution prior to FACS analysis.

Immunostained cells were analyzed with a FACS Canto II flow cytometer (BD Bioscience, San Jose, CA). Single cells were selected based their light scattering area and width profiles. 2500 transfected cells expressing PMP22 were analyzed from each sample by gating on GFP-positive cells (excited with a 488 nm laser, detected with 515−545 nm emission filter). The single-cell PE intensity (surface PMP22, excited with a 488 nm laser, detected with 564−606 nm emission filter) and Alexa Fluor 647 intensity (internal PMP22, excited with a 633 nm laser, detected with 650−670 nm emission filter) signals were corrected for nonspecific binding by subtracting the average intensities of untransfected, GFP-negative cells within each sample. To correct for the difference in the fluorescence intensity of the two antibodies, cells expressing WT PMP22 were stained with either the PE-labeled antibody or the Alexa Fluor 647-labeled antibody prior to FACS analysis, and the ratio of the average intensities of these cells was used to normalize the two signals. Single-cell trafficking efficiency values were then calculated from the ratio of the corrected PE signal of a given cell over the sum of its corrected Alexa Fluor 647 and PE signals. Average trafficking efficiency values calculated in this fashion were found to be similar to those determined by a comparison of the population-averaged intensities of intact (surface PMP22) and permeabilized (total PMP22) cells stained with the same concentration of the same fluorescently labeled antibody. Single-cell fluorescence intensity values below the background intensity were assigned an intensity of 0. Cells for which this correction or for which extremely low intensity values resulted in a nonreal or artificially inflated efficiency ratio (>50% efficiency, typically less than 1% of the population) were discarded from the analysis. Results were analyzed and visualized using FlowJo X software (Treestar Inc., Ashland, OR).

From titrations of both intact and permeable cells expressing WT PMP22 with fluorescently labeled antibodies, we found the average fluorescence intensity to be linearly dependent upon the antibody concentration. This confirms that fluorescence intensity values fall within the linear range of the detectors. Moreover, this ensures that the observed trafficking efficiency values are independent of the chosen antibody concentration. Compensation for spillover of the fluorescence signals between the channels utilized for the analysis as well as the gates for the selection of single cells, GFP-positive cells, and GFP-negative cells was initially set manually but was kept consistent for the collection of all data sets obtained thereafter.

■ ASSOCIATED CONTENT

S Supporting Information

Near-UV CD spectra of PMP22 variants at equilibrium in DPC micelles and in denaturing mixed micelles. Zn(II) binding of S22F PMP22. Tryptophan emission spectrum of G107V at physiological pH. Plot of cellular trafficking against the energetic effects of mutations on the folding of the PMP22 apoprotein. Supplemental theory section detailing the thermodynamic correction of apparent binding energetics and simulated effects of binding on folding. Table of motor nerve conduction velocities of heterozygous patients carrying mutations in the *PMP22* gene. Table of observed Zn(II) binding kinetics for PMP22 variants. The Supporting Information is available free of charge on the ACS Publications website at DOI: 10.1021/jacs.5b03743.

■ AUTHOR INFORMATION

Corresponding Author
*chuck.sanders@vanderbilt.edu

Notes
The authors declare no competing financial interest.

■ ACKNOWLEDGMENTS

■ REFERENCES

(1) Schubert, U.; Anton, L. C.; Gibbs, J.; Norbury, C. C.; Yewdell, J. W.; Bennink, J. R. *Nature* **2000**, *404*, 770−774.
(2) Kowalski, J. M.; Parekh, R. N.; Wittrup, K. D. *Biochemistry* **1998**, *37*, 1264−1273.
(3) Kowalski, J. M.; Parekh, R. N.; Mao, J.; Wittrup, K. D. *J. Biol. Chem.* **1998**, *273*, 19453−19458.
(4) Sekijima, Y.; Wiseman, R. L.; Matteson, J.; Hammarstrom, P.; Miller, S. R.; Sawkar, A. R.; Balch, W. E.; Kelly, J. W. *Cell* **2005**, *121*, 73−85.
(5) Calloni, G.; Zoffoli, S.; Stefani, M.; Dobson, C. M.; Chiti, F. *J. Biol. Chem.* **2005**, *280*, 10607−10613.
(6) Mayer, S.; Rudiger, S.; Ang, H. C.; Joerger, A. C.; Fersht, A. R. *J. Mol. Biol.* **2007**, *372*, 268−276.
(7) Reich, L.; Becker, M.; Seckler, R.; Weikl, T. R. *Biophys Chem.* **2009**, *141*, 186−192.
(8) Schlebach, J. P.; Sanders, C. R. *Q. Rev. Biophys.* **2014**, 1−35.
(9) Sanders, C.; Myers, J. *Annu. Rev. Biophys. Biomol. Struct.* **2004**, *33*, 25−51.
(10) Ng, D. P.; Poulsen, B. E.; Deber, C. M. *Biochim. Biophys. Acta* **2012**, *1818*, 1115−1122.
(11) Guerriero, C. J.; Brodsky, J. L. *Physiol Rev.* **2012**, *92*, 537−576.
(12) Ruggiano, A.; Foresti, O.; Carvalho, P. *J. Cell Biol.* **2014**, *204*, 869−879.
(13) Li, J.; Parker, B.; Martyn, C.; Natarajan, C.; Guo, J. *Mol. Neurobiol.* **2013**, *47*, 673−698.
(14) Naef, R.; Suter, U. *Neurobiol. Dis.* **1999**, *6*, 1−14.
(15) Notterpek, L.; Ryan, M. C.; Tobler, A. R.; Shooter, E. M. *Neurobiol. Dis.* **1999**, *6*, 450−460.
(16) Jetten, A. M.; Suter, U. *Prog. Nucleic Acid Res. Mol. Biol.* **2000**, *64*, 97−129.
(17) Pareek, S.; Suter, U.; Snipes, G. J.; Welcher, A. A.; Shooter, E. M.; Murphy, R. A. *J. Biol. Chem.* **1993**, *268*, 10372−10379.
(18) Pareek, S.; Notterpek, L.; Snipes, G. J.; Naef, R.; Sossin, W.; Laliberté, J.; Iacampo, S.; Suter, U.; Shooter, E. M.; Murphy, R. A. *J. Neurosci.* **1997**, *17*, 7754−7762.
(19) Colby, J.; Nicholson, R.; Dickson, K. M.; Orfali, W.; Naef, R.; Suter, U.; Snipes, G. J. *Neurobiol. Dis.* **2000**, *7*, 561−573.
(20) Tobler, A. R.; Liu, N.; Mueller, L.; Shooter, E. M. *Proc. Natl. Acad. Sci. U. S. A.* **2002**, *99*, 483−488.
(21) Schlebach, J. P.; Peng, D.; Kroncke, B. M.; Mittendorf, K. F.; Narayan, M.; Carter, B. D.; Sanders, C. R. *Biochemistry* **2013**, *52*, 3229−3241.
(22) Tobler, A. R.; Notterpek, L.; Naef, R.; Taylor, V.; Suter, U.; Shooter, E. M. *J. Neurosci.* **1999**, *19*, 2027−2036.
(23) Schlebach, J. P.; Sanders, C. R. *J. Membr. Biol.* **2014**, DOI: 10.1007/s00232-014-9726-0.
(24) Myers, J. K.; Mobley, C. K.; Sanders, C. R. *Biochemistry* **2008**, *47*, 10620−10629.
(25) Kelly, J. W.; Balch, W. E. *Nat. Chem. Biol.* **2006**, *2*, 224−227.
(26) Wiseman, R. L.; Powers, E. T.; Buxbaum, J. N.; Kelly, J. W.; Balch, W. E. *Cell* **2007**, *131*, 809−821.
(27) Powers, E. T.; Morimoto, R. I.; Dillin, A.; Kelly, J. W.; Balch, W. E. *Annu. Rev. Biochem.* **2009**, *78*, 959−991.
(28) Viquez, O. M.; Lai, B.; Ahn, J. H.; Does, M. D.; Valentine, H. L.; Valentine, W. M. *Toxicol. Appl. Pharmacol.* **2009**, *239*, 71−79.
(29) Frederickson, C. J. *Int. Rev. Neurobiol.* **1989**, *31*, 145−238.
(30) Popot, J. L.; Trewhella, J.; Engelman, D. M. *EMBO J.* **1986**, *5*, 3039−3044.
(31) Dickson, K. M.; Bergeron, J. J.; Shames, I.; Colby, J.; Nguyen, D. T.; Chevet, E.; Thomas, D. Y.; Snipes, G. J. *Proc. Natl. Acad. Sci. U. S. A.* **2002**, *99*, 9852−9857.
(32) Fontanini, A.; Chies, R.; Snapp, E. L.; Ferrarini, M.; Fabrizi, G. M.; Brancolini, C. *J. Biol. Chem.* **2005**, *280*, 2378−2387.
(33) Ryan, M. C.; Shooter, E. M.; Notterpek, L. *Neurobiol. Dis.* **2002**, *10*, 109−118.
(34) Mittendorf, K. F.; Kroncke, B. M.; Meiler, J.; Sanders, C. R. *Biochemistry* **2014**, *53*, 6139−6141.
(35) Kumar, N.; Gross, J. B., Jr.; Ahlskog, J. E. *Neurology* **2004**, *63*, 33−39.
(36) Terril-Robb, L. A.; Clemons, D. J.; Besch-Williford, C.; O'Brien, D. P.; O'Dell, B. L. *Proc. Soc. Exp Biol. Med.* **1996**, *213*, 50−58.
(37) Unal, B.; Tan, H.; Orbak, Z.; Kiki, I.; Bilici, M.; Bilici, N.; Aslan, H.; Kaplan, S. *Brain Res.* **2005**, *1048*, 228−234.
(38) Inouye, H.; Kirschner, D. A. *Biochim. Biophys. Acta* **1984**, *776*, 197−208.
(39) Kursula, P.; Mariläinin, G.; Lehto, V.; Heape, A. M. *J. Neurochem.* **1999**, *73*, 2110−2118.
(40) Bund, T.; Boggs, J. M.; Harauz, G.; Hellmann, N.; Hinderberger, D. *Biophys. J.* **2010**, *99*, 3020−3028.
(41) Smith, G. S.; Chen, L.; Bamm, V. V.; Dutcher, J. R.; Harauz, G. *Amino Acids* **2010**, *39*, 739−750.
(42) Liu, P. F.; Park, C. *J. Mol. Biol.* **2012**, *422*, 403−413.
(43) Sakakura, M.; Hadziselimovic, A.; Wang, Z.; Schey, K. L.; Sanders, C. R. *Structure* **2011**, *19*, 1160−1169.
(44) Jung, J.; Coe, H.; Michalak, M. *FASEB J.* **2011**, *25*, 3929−3937.
(45) Fortun, J.; Go, J. C.; Li, J.; Amici, S. A.; Dunn, W. A.; Notterpek, L. *Neurobiol. Dis.* **2006**, *22*, 153−164.
(46) Fortun, J.; Dunn, W. A.; Joy, S.; Li, J.; Notterpek, L. *J. Neurosci.* **2003**, *23*, 10672−10680.
(47) Fortun, J.; Li, J.; Go, J.; Fenstermaker, A.; Fletcher, B. S.; Notterpek, L. *J. Neurochem* **2005**, *92*, 1531−1541.
(48) Kopito, R. R. *Trends Cell Biol.* **2000**, *10*, 524−530.
(49) Bernier, V.; Lagace, M.; Bichet, D. G.; Bouvier, M. *Trends Endocrin Met* **2004**, *15*, 222−228.
(50) Hanrahan, J. W.; Sampson, H. M.; Thomas, D. Y. *Trends Pharmacol. Sci.* **2013**, *34*, 119−125.
(51) Maya-Nunez, G.; Ulloa-Aguirre, A.; Janovick, J. A.; Conn, P. M. *Subcell. Biochem.* **2012**, *63*, 263−289.

(52) Tzekov, R.; Stein, L.; Kaushal, S. *Cold Spring Harbor Perspect. Biol.* **2011**, *3*, a007492.

(53) Wang, Y.; Wrennall, J. A.; Cai, Z.; Li, H.; Sheppard, D. N. *Int. J. Biochem. Cell Biol.* **2014**, *52*, 47−57.

(54) Bichet, D. G. *Semin. Nephrol.* **2008**, *28*, 245−251.

(55) Partridge, A. W.; Therien, A. G.; Deber, C. M. *Proteins* **2004**, *54*, 648−656.

(56) Partridge, A. W.; Therien, A. G.; Deber, C. M. *Biopolymers* **2002**, *66*, 350−358.

(57) Rader, A. J.; Anderson, G.; Isin, B.; Khorana, H. G.; Bahar, I.; Klein-Seetharaman, J. *Proc. Natl. Acad. Sci. U. S. A.* **2004**, *101*, 7246−7251.

(58) Almqvist, J.; Huang, Y.; Hovmoller, S.; Wang, D. N. *Biochemistry* **2004**, *43*, 9289−9297.

(59) Therien, A. G.; Grant, F. E.; Deber, C. M. *Nat. Struct. Biol.* **2001**, *8*, 597−601.

(60) Cheung, J. C.; Deber, C. M. *Biochemistry* **2008**, *47*, 1465−1473.

(61) Mobley, C. K.; Myers, J. K.; Hadziselimovic, A.; Ellis, C. D.; Sanders, C. R. *Biochemistry* **2007**, *46*, 11185−11195.

(62) Liu, N.; Yamauchi, J.; Shooter, E. M. *Neurobiol. Dis.* **2004**, *17*, 300−309.

(63) Robben, J. H.; Sze, M.; Knoers, N. V.; Deen, P. M. *Mol. Biol. Cell* **2006**, *17*, 379−386.